Optical determination of the electronic coupling and intercalation geometry of thiazole orange homodimer in DNA

Citation: Cunningham, Paul D., William P. Bricker, Sebastián A. Díaz, Igor L. Medintz, Mark Bathe, and Joseph S. Melinger. "Optical Determination of the Electronic Coupling and Intercalation Geometry of Thiazole Orange Homodimer in DNA." The Journal of Chemical Physics 147, no. 5 (August 7, 2017): 055101. © 2018 AIP Publishing LLC

As Published: https://doi.org/10.1063/1.4995431

Publisher: American Institute of Physics (AIP)

Persistent URL: http://hdl.handle.net/1721.1/119630

Version: Final published version: final published article, as it appeared in a journal, conference proceedings, or other formally published context

Optical determination of the electronic coupling and intercalation geometry of thiazole orange homodimer in DNA

Paul D. Cunningham, William P. Bricker, Sebastián A. Díaz, Igor L. Medintz, Mark Bathe, and Joseph S. Melinger

Citation: The Journal of Chemical Physics **147**, 055101 (2017); doi: 10.1063/1.4995431
View online: https://doi.org/10.1063/1.4995431
View Table of Contents: http://aip.scitation.org/toc/jcp/147/5
Published by the American Institute of Physics

Optical determination of the electronic coupling and intercalation geometry of thiazole orange homodimer in DNA

Paul D. Cunningham,[1] William P. Bricker,[2] Sebastián A. Díaz,[3] Igor L. Medintz,[3] Mark Bathe,[2] and Joseph S. Melinger[1,a)]
[1]*Electronics Science and Technology Division, U.S. Naval Research Laboratory, Washington, DC 20375-5320, USA*
[2]*Department of Biological Engineering, Massachusetts Institute of Technology, Cambridge, Massachusetts 02139, USA*
[3]*Center for Bio/Molecular Science and Engineering, U.S. Naval Research Laboratory, Washington, DC 20375-5320, USA*

(Received 12 March 2017; accepted 10 July 2017; published online 4 August 2017)

Sequence-selective bis-intercalating dyes exhibit large increases in fluorescence in the presence of specific DNA sequences. This property makes this class of fluorophore of particular importance to biosensing and super-resolution imaging. Here we report ultrafast transient anisotropy measurements of resonance energy transfer (RET) between thiazole orange (TO) molecules in a complex formed between the homodimer TOTO and double-stranded (ds) DNA. Biexponential homo-RET dynamics suggest two subpopulations within the ensemble: 80% intercalated and 20% non-intercalated. Based on the application of the transition density cube method to describe the electronic coupling and Monte Carlo simulations of the TOTO/dsDNA geometry, the dihedral angle between intercalated TO molecules is estimated to be 81° ± 5°, corresponding to a coupling strength of 45 ± 22 cm^{-1}. Dye intercalation with this geometry is found to occur independently of the underlying DNA sequence, despite the known preference of TOTO for the nucleobase sequence CTAG. The non-intercalated subpopulation is inferred to have a mean inter-dye separation distance of 19 Å, corresponding to coupling strengths between 0 and 25 cm^{-1}. This information is important to enable the rational design of energy transfer systems that utilize TOTO as a relay dye. The approach used here is generally applicable to determining the electronic coupling strength and intercalation configuration of other dimeric bis-intercalators. [http://dx.doi.org/10.1063/1.4995431]

I. INTRODUCTION

Dimeric cyanine dyes are often used for DNA staining applications because of their tendency to intercalate between the DNA base pairs. Among the more popular bis-intercalating cyanine dyes are the thiazole orange (TO) and oxazole yellow (YO) homodimers called TOTO and YOYO, respectively. These intercalating dimers exhibit strong binding affinities ~1 nM and a relatively large, ~1000-fold, increase in fluorescence in the presence of DNA,[1,2] which makes these dyes a versatile and powerful type of molecular beacon for biotechnology and other applications. This increase in fluorescence occurs because intercalation inhibits rotational motion about the methine bridge, thereby suppressing the isomerization that leads to a non-fluorescent excited state. Also, the binding to DNA greatly attenuates the formation of non-fluorescent H-aggregates, which can occur when TOTO and YOYO are free in aqueous solution. This property also makes this class of fluorophore particularly valuable for applications in fluorescent labeling[2,3] and super-resolution imaging.[4,5]

Our interest in these intercalating dimers stems from their possible use in DNA-organized chromophore arrays for light-harvesting and nanoscale energy transfer. As a related example, intercalating YO monomers have been self-assembled within a DNA duplex to serve as a relay wire to achieve long-range energy transfer through homo-resonance energy transfer (RET) interactions.[6,7] The cyanine dimers have attractive photophysical properties for controlling energy transfer; however, their usefulness in DNA-organized light harvesting networks has not yet been well explored. First, the cyanine dimers have high peak molar absorptivity, in excess of 10^5 M^{-1} cm^{-1},[1] and when bound to DNA, they exhibit reasonably high fluorescence quantum yields in the range of 35%-40%.[8] These properties are attractive for relay fluorophores in energy transfer networks, which must function as both donor and acceptor. Second, the TOTO dimer has been found to show sequence-selective binding to dsDNA with a ~100-fold preference for binding to CTAG sequence over any other sequence present in the dsDNA.[9] Since that work, other nucleobase sequences, involving inosine and methylcytosine, have been identified that show even higher sequence-selective TOTO intercalation.[10] This sequence-selectivity suggests that the RET properties of a DNA energy transfer network may be tuned by strategic placement of nucleobase sequences with high TOTO affinity and specificity.

a)Author to whom correspondence should be addressed: joseph.melinger@nrl.navy.mil

To better assess the potential of TOTO to function in energy transfer designs using programmed DNA scaffolds, it is important to understand the nature of the energy transfer between the TO fluorophores. This is the main goal of the current work. The energy transfer rate, in turn, may depend on environmental factors such as the presence of a site-specific sequence for TOTO binding or the type of buffer used to stabilize the TOTO/DNA complex. The most accurate information regarding the geometric configuration of the TOTO/DNA complex to date comes from nuclear magnetic resonance (NMR) spectroscopy[11] and is shown in Fig. 1. The TOTO dimer represents an interesting case for the description of energy transfer because the relatively close separation of the TO molecules, ~9.6 Å, is similar to the length of the TO fluorophore itself, ~10.8 Å. In such situations, it is important to consider the geometry of the TO transition density,[12] rather than use the Point Dipole Approximation (PDA), in order to understand the strength of the electronic coupling and rate of energy transfer in TOTO. While such short separations between cyanine fluorophores often produce excitonic interactions,[13] the near orthogonal dihedral angle between the TO molecules attenuates the electronic coupling. For nearly orthogonal TO molecules, the electronic coupling and energy transfer rate become highly sensitive to the precise value of the dihedral angle.[14] Thus, the details of the energy transfer kinetics provide a measure of the disorder in the dihedral angle when TOTO intercalates into dsDNA.

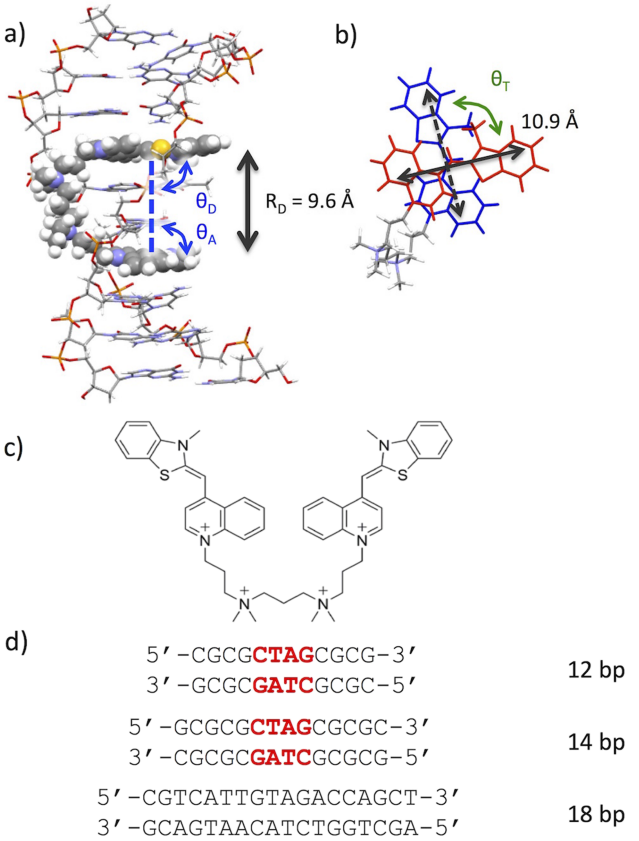

FIG. 1. (a) Side view of the geometric configuration of TOTO/DNA complex from the Protein Data Bank[18] (PDB ID: 108D),[11] with donor-acceptor distance R_{DA} and angles θ_D and θ_A indicated, (b) top view of the same TOTO configuration, where the DNA is omitted for clarity, with length and dihedral angle θ_T indicated, (c) chemical structure of the TOTO dimer generated using ChemDraw, and (d) dsDNA sequences used in the measurements. The CTAG site is highlighted in red.

In the present work, we explore the optical and energy transfer properties of the TOTO/DNA complex using a combination of steady-state absorption and fluorescence, time-resolved fluorescence, and ultrafast pump-probe anisotropy. To evaluate the sensitivity of the optical and energy transfer properties of TOTO to environmental factors, measurements were performed in the presence and absence of the CTAG sequence and were compared in three different buffer solutions: phosphate buffered saline (PBS), tris-acetate-ethylenediaminetetraacetic acid (TAE), and 3-[tris-(hydroxymethyl)methylamino]-1-propanesulfonic acid—tetrapentylammonium (TAPS, also known as TAPS-NPe_4^+). The TAPS buffer, in particular, has been shown to promote tighter TOTO binding to dsDNA.[15] Energy transfer is analyzed using the PDA as well as the transition density cube (TDC) method of calculating the electronic coupling between TO fluorophores. Experimentally, we find that both the optical properties and the energy transfer kinetics are remarkably insensitive to the presence/absence of the CTAG sequence and type of buffer environment. Ultrafast anisotropy measurements reveal a biexponential rate of energy equilibration between the TO molecules. These two distributions of decay times suggest the coexistence of two TOTO configurations, intercalated and non-intercalated subpopulations, consistent with recent work, suggesting that intercalation is a dynamic process in equilibrium with other bound yet non-intercalated geometries.[16] Our results are consistent with previous ultrafast anisotropy measurements of the YOYO/DNA complex;[17] however, the TOTO/DNA complex shows an average energy transfer rate that is approximately 1.5 times higher. Through Monte Carlo simulations of these results, we estimate the dihedral angle of the intercalated TOTO and the inter-dye separation for the non-intercalated subpopulation.

II. METHODS AND MATERIALS

Synthetic single-stranded (ss) DNA with custom sequences was purchased from Integrated DNA Technologies, Inc. (IDT) to self-assemble into dsDNA duplexes of length 12 and 14 base pair (bp) with sequences identical to those used by Spielmann *et al.*[11] Each duplex contains one CTAG site, Fig. 1. Additionally, we compare to an 18 bp dsDNA duplex (purchased from IDT) without the CTAG site, which was readily available in our lab. Samples were prepared and characterized in three different buffer solutions: PBS, TAE, and TAPS. The following buffer compositions were used: 2.5× PBS—350 mM NaCl, 6.75 mM KCl, 25 mM $Na_2H_2PO_4$, 1.8 mM KH_2PO_4; TAE–40 mM TRIS, 20 mM acetic acid, and 1 mM ethylenediaminetetraacetic acid (EDTA); TAPS, also known as TAPS-NPE_4^+, was prepared based on Ref. 15 by titrating 40 mM 3-[tris-(hydroxymethyl)methylamino]-1-propanesulfonic acid and 1 mM EDTA with tetrapentyl ammonium hydroxide until the pH reaches 8.2. Because TAPS buffer has been shown to further stabilize the binding of TOTO to dsDNA,[15] it seemed reasonable to expect some variations in spectroscopic properties of the TOTO/dsDNA

complex in these different solutions. Unless otherwise stipulated, the concentration of the TOTO/dsDNA complex in the buffer solutions was typically ~3 μM, with a 1:1 TOTO:DNA concentration ratio.

Steady-state absorption spectra were measured for 150 μl samples in a 1 cm path length cuvette using an Agilent 8453 diode array UV-vis spectrophotometer. Fluorescence spectra and fluorescence excitation profiles, corrected for the wavelength response of the lamp, grating, and detector, were measured using a Multifunction Microtiter Plate Reader (Tecan Infinite MR 1000 Pro).

Fluorescence lifetimes were measured on 3 μM samples in a 1 mm path cuvette using the time-correlated single photon counting (TCSPC) technique. The system[19] was based on an 80 MHz 7 ps pulses 532 nm frequency-doubled diode-pumped Nd:YVO_4 laser (High-Q picoTRAIN). A micro channel plate photomultiplier tube (Hamamatsu) was used to detect the fluorescence with an instrument response full width at half maximum (FWHM) of approximately 45 ps.

Ultrafast transient absorption spectroscopy was used to measure the excited state dynamics of ~250 μl samples (~3 μM) in a 1 cm stirring cuvette maintained at a temperature of 283 K (10 °C) to avoid potential sample degradation from laser induced heating. The experimental setup[20] was based on a 1 kHz 1 W 150 fs pulsed Ti:sapphire amplifier (CPA 2101, Clark-MXR). The output is split with approximately 300 mW used to pump a non-collinear visible optical parametric amplifier to produce tunable excitation pulses. A half wave plate is used to control the relative polarization of the excitation beam. A small amount of power is focused onto a sapphire plate to generate the linearly polarized white light continuum probe. The white light pulses are then sent into a scanning monochromator to record the excited state spectra. An instrument response with FWHM of 400 fs was measured via two-photon absorption in ZnSe.

III. RESULTS AND DISCUSSION

The absorption spectra for 1:1 TOTO:dsDNA do not show the high energy excitonic peak associated with H-aggregates that form when free TOTO in solution dimerizes,[1] or any signs of forming other excited state complexes,[21] see Fig. 2(a) and Fig. S1 of the supplementary material. There were no significant changes to the absorption spectra for more concentrated solutions 10 μM 1:1 TOTO:dsDNA (not shown). Because H-aggregates are not fluorescent, if present their effects will appear in absorption spectra but will be absent from fluorescence excitation spectra. We observe agreement between the absorption and fluorescence excitation spectra, Fig. 2(a), again indicating the absence of H-aggregates. Together this suggests that for 1:1 TOTO:dsDNA, nearly all of the TOTO bind to the dsDNA duplex, potentially via intercalation, which is known to be the preferred binding mode, to form fluorescent species. The similarity between the absorption and fluorescence excitation spectra also indicates that the TO molecules do not couple strongly enough to produce clear excitonic features in the absorption spectrum.[13,21,22] Further, the similarity of the absorption, excitation, and fluorescence spectra collected in three different buffer solutions, TAE, TAPS, and PBS, Fig. S1, also supports that the different counter cations in these buffer solutions all favor TOTO intercalation.

Measurement of the excited state lifetime, Fig. 2(b), can provide a more sensitive test of the homogeneity of TOTO binding. The fluorescence decays for TOTO-dsDNA are essentially the same in all three buffers, Fig. S1 of the supplementary material. The coefficients of the best fits to the fluorescence decays are shown in Table S1 of the supplementary material. Nearly single exponential luminescence decay lifetimes (~2.5 ns) indicate suppressed rotation about the methine bridge of the TO molecule, which indicates that most of the TOTO have intercalated. However, in each case, a relatively small

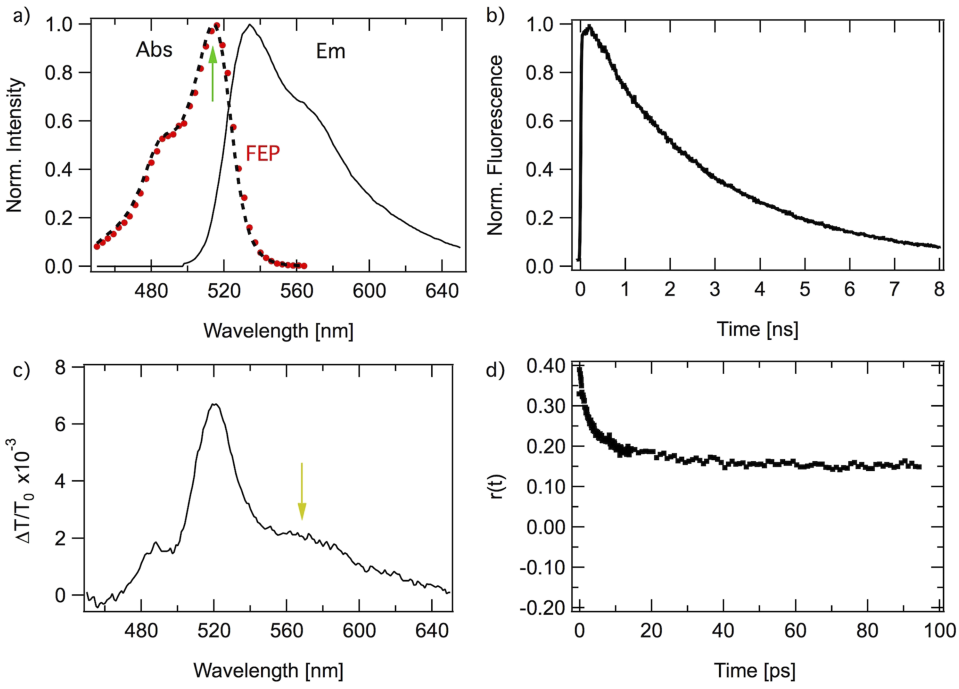

FIG. 2. Representative (a) absorption (black, dashed), fluorescence excitation profile (red, dotted), and emission (black, solid) spectra, (b) time-resolved fluorescence decay, (c) transient absorption spectrum, and (d) anisotropy dynamics of 1:1 TOTO:dsDNA in PBS. The 513 nm excitation (green) and 568 nm probe (yellow) wavelengths used to measure the transient absorption anisotropy dynamics are indicated by arrows.

percentage (~10%-18%) of a second component with a shorter lifetime is needed to reproduce the decay curves. One possible explanation of the biexponential decays is that there is a minor contribution from a second binding geometry to the dsDNA, in which rotations of the TO molecule are only partly suppressed. This possibility is explored in more detail below.

The anisotropy dynamics recovered from polarized ultrafast transient absorption measurements provide insight into the electronic coupling between TO molecules. Here, the TOTO is photoexcited at 513 nm near its absorption maximum. The transient absorption spectrum, Fig. 2(c), is composed of overlapping ground state bleach and stimulated emission bands and therefore resembles the sum of the absorption and emission bands. No evidence of photoinduced electron transfer was observed. Polarization sensitive measurements were made for a probe wavelength of 568 nm, which corresponds to the low energy shoulder of the stimulated emission band. The time-resolved anisotropy was calculated as[23]

$$r(t) = \frac{\Delta T_{para} - \Delta T_{perp}}{\Delta T_{para} + 2\Delta T_{perp}}, \tag{1}$$

where ΔT_{para} and ΔT_{perp} are the photoinduced changes in transmission for mutually parallel and perpendicular polarizations, respectively. For TOTO, the picosecond scale decay of the anisotropy, Fig. 2(d), is due to energy transfer between TO molecules, which depolarizes the initial photoselected state because of the different orientations of the two TO molecules. As intercalation hinders the motion of each TO, rotational depolarization is dominated by tumbling of the DNA and occurs on a nanosecond time scale.

Similar anisotropy decay dynamics were observed for TOTO/dsDNA in PBS, TAE, and TAPS buffer solutions, Fig. S2 of the supplementary material. On average, the anisotropy dynamics show a biexponential decay from 0.37 ± 0.03 to 0.14 ± 0.02. Because the TOTO/dsDNA in solution is randomly oriented, photoselection with a polarized light field is expected to produce an initial anisotropy of 0.4.[23,24] The residual anisotropy value after energy transfer depends on the relative orientation of the two TO molecules. When fit with biexponential functions, the decay times are 1.9 ± 0.3 ps and 16 ± 5 ps, with approximately 20% of the intensity weighted towards the slower time constant. The observed dynamics did not change significantly for 1:1 TOTO:dsDNA solution concentrations between 2 μM and 10 μM, Fig. S3 of the supplementary material. Similar biexponential anisotropy dynamics have been previously reported for the bis-intercalator YOYO,[17] though with approximately 1.5 × slower time constants, indicating weaker electronic coupling in YOYO than in TOTO. Inhomogeneity in dye position[25] or orientation[26] can give rise to deviations from single exponential RET dynamics. For bis-intercalators, a subpopulation of bound but not fully intercalated dye can coexist with the intercalated dye[16] and may give rise to the observed biexponential RET dynamics.

The anisotropy decay dynamics yield an estimate of coupling between the individual TO molecules of TOTO intercalated into dsDNA. For homo-RET, the time-dependent anisotropy[27] is related to the RET rate by

$$r(t) = r_0\left(\frac{1+e^{-2k_{ET}t}}{2} + \frac{1-e^{-2k_{ET}t}}{2} d(\theta_T, \theta_D, \theta_A)\right), \tag{2}$$

where the depolarization factor can be approximated for coplanar molecules as

$$d(\theta_T, \theta_D, \theta_A) \approx d(\theta_T) = \frac{1}{2}\left(3\cos^2\theta_T - 1\right). \tag{3}$$

The three angles are specified between the donor and acceptor (θ_T), between the donor and the vector connecting the two dyes (θ_D), and between the acceptor and the vector connecting the two dyes (θ_A), see Fig. 1. The energy transfer, k_{ET}, rate can be expressed as a function of the electronic coupling,[28] V, as

$$k_{ET} = \frac{2\pi}{\hbar}|V|^2 J_{DA}, \tag{4}$$

where J_{DA} is the spectral overlap integral and is calculated as[12]

$$J_{DA} = \frac{1}{h}\int \frac{C_D f_D(\nu)}{\nu^3}\frac{C_A \varepsilon_A(\nu)}{\nu} d\nu, \tag{5}$$

where υ is the frequency, $f_D(\upsilon)$ is the fluorescence spectrum of the donor, $\varepsilon_A(\upsilon)$ is the molar absorptivity of the acceptor, and $C_{D,A}$ are normalization factors such that the integrals over each term are unity. We assume that the electronic coupling, V, consists solely of long-range Coulombic interaction and that any short-range exchange interactions are negligible at these inter-chromophore distances.[28] For the TOTO dimer, the overlap integral was calculated to be 4.02×10^{18} J^{-1} using Eq. (5) and spectroscopic measurements of the TOTO molar absorptivity and fluorescence spectrum. When applying the PDA, we approximate the electronic coupling as a dipole-dipole coupling[29] between transition dipole moments located at the center of charge of the transition density of the molecules,

$$V \approx V_{PDA} = \frac{\kappa\left|\vec{\mu}_D\right|\left|\vec{\mu}_A\right|}{4\pi\varepsilon_0 n^2 R_{DA}^3}, \tag{6}$$

where ε_0 is the permittivity of free space, n is the refractive index, R_{DA} is the donor-acceptor separation distance, and $\vec{\mu}_{D,A}$ is the transition dipole moment of the donor or acceptor, respectively. The orientation factor,[30] κ, is expressed as

$$\kappa = \hat{\mu}_D \cdot \hat{\mu}_A - 3\left(\hat{\mu}_D \cdot \hat{R}_{DA}\right)\left(\hat{\mu}_A \cdot \hat{R}_{DA}\right). \tag{7}$$

Here the three dot products are the cosines of θ_T, θ_D, and θ_A, respectively, see Fig. 1. From Eqs. (3) and (7), both the time-dependent anisotropy and the energy transfer rate will depend on the dihedral angle of the intercalating TOTO or θ_T.

From Eq. (2), the observed anisotropy decay is expressed as a single exponential function with decay rate equal to twice the RET rate. However, we observe at least two decay times from TOTO/dsDNA regardless of buffer solution. From Eq. (4), we estimate the dipole coupling as 50 ± 4 cm^{-1} and 17 ± 3 cm^{-1} from the fast and slow components of the anisotropy decay, respectively. This suggests that more than one configuration is present when TOTO interacts with dsDNA. Considering only intercalation, the dihedral angles implied by these weak-to-moderate coupling strengths suggest nearly orthogonal TO molecules. This is inconsistent with the measured initial and final anisotropy, which suggest a more moderate dihedral angle near 66°. This inconsistency may be related to the application of the PDA, which by way of overestimating the coupling for a given dihedral angle may

erroneously point toward near orthogonal dyes. This inconsistency may also point to the violation of our assumption that all of the TOTO intercalate completely. Both possibilities are investigated below.

Intercalation between the C-G and T-A and the A-T and G-C of the CTAG site implies that the TO molecules are less than 10 Å apart. In order to accommodate the intercalating dye, the DNA undergoes conformational changes. Based on NMR studies, the DNA strand lengthens and unwinds to increase the separation distance between base pairs.[31] The NMR studies suggest that these changes lead to a separation distance of 9.6 Å between the TO molecules.[11] This separation is less than the extent of each individual TO molecule along its long axis (~10.6 Å). When in such close proximity, the electronic coupling between donor and acceptor becomes dominated by local interactions between the edges of the transition densities, and the failure of the PDA leads to overestimation of the electronic coupling.[13] Departure from the PDA may be more pronounced for static molecules, like bis-intercalators, because orientational averaging for dyes attached with long flexible linkers can partially cancel these errors.[12]

To more accurately estimate the electronic coupling, we employed the TDC method, which better approximates the electronic coupling by discretizing the transition densities onto a volumetric grid.[32,33] The electronic coupling using the TDC method is represented as

$$V \approx V_{TDC} = \sum_{i,j} \frac{M_D(i)\, M_A(j)}{4\pi\varepsilon_0 r_{ij}}, \tag{8}$$

where $M_{D,A}$ represents the discretized transition densities calculated from the ground (Ψ_{GS}) and excited state (Ψ_{ES}) wavefunctions of the donor (D) and acceptor (A) dye molecules,

$$M_{D,A}(x,y,z) = V_\delta \int_z^{z+\delta_z} \int_y^{y+\delta_y} \int_x^{x+\delta_x} \Psi_{GS} \Psi_{ES}^* \mathrm{d}x\mathrm{d}y\mathrm{d}z, \tag{9}$$

with grid size, δ, and volume element, V_δ.

The TOTO transition densities are calculated using time-dependent density functional theory[34,35] (TD-DFT) using the CAM-B3LYP functional[36] with the 6-31+G(d) basis set,[37,38] as implemented in the NWChem 6.6 software package.[39] The structure determined from NMR studies in the literature and stored in the Protein Data Bank[18] (PDB ID: 108D)[11] is used as a starting configuration for quantum chemical modeling. To generate a starting configuration for TOTO, we choose the first model from the NMR data, which was solved using a B-form DNA starting structure. The first NMR model has a dihedral angle and electronic couplings close to the mean of the sample of twenty structures, as seen in Fig. S4 and Tables S2 and S3 of the supplementary material, making it acceptable as a representative starting configuration. The TOTO molecules in this model are separated by two base pairs resulting in a center-to-center separation distance of 9.6 Å and a dihedral angle of 78°. Next, for TD-DFT modeling, the TOTO molecule is split into donor and acceptor TO molecules [Fig. S5(b) of the supplementary material] since the alkyl-amino linker likely contributes only to binding affinity of TOTO to dsDNA and not to energy transfer. To do this, the alkyl-amino linker between TO molecules is removed, and a methyl group is instead attached to the charged amine group. Using these initial configurations, the $S_0 \rightarrow S_1$ energies and transition dipole moments of the TOTO molecules were calculated using TD-DFT as shown in Table S2, as well as the transition densities shown in Fig. S5. The estimated transition energy for this initial configuration is larger than the observed value of 2.4 eV, and the calculated dipole moment is smaller than the 8 D value estimated from the TOTO absorption spectrum. The dipole coupling is estimated from a modified version of Eq. (4) with the Lorentz factor $\left(f_L^2 = 1.57\right)$ in the numerator and n^2 in the denominator. Because these calculations are carried out in vacuum, they tend to underestimate the dipole moments. Therefore, the results are scaled to match the 8 D transition dipole moment estimated from the TOTO absorption spectrum, as shown in Table S3 of the supplementary material. From the PDA, we know that changes in dihedral angle dominate the dipole coupling as compared with small changes in the donor acceptor separation distance and deviations from the assumed coplanar geometry. Keeping the donor-acceptor separation fixed at 9.6 Å, the TDC calculation was performed as a function of dihedral angle to estimate the dependence of the electronic coupling on dihedral angle, Fig. 3. A script utilizing the Python package ProDy[40] performed the TOTO molecule coordinate transformations necessary for these TDC calculations. For consistency, the dihedral angle here is defined as the angle between the transition dipole moments. Both the PDA and TDC calculations of the electronic coupling show the expected $A\,|\cos(\theta + \phi)|$ dependence on dihedral angle. Best fits to the data yield $A = 324\ \mathrm{cm}^{-1}$ and $\phi = 0.5°$ for the PDA and $A = 188\ \mathrm{cm}^{-1}$ and $\phi = -4.6°$ for the TDC. The PDA overestimated the electronic coupling for nearly all orientations. There is also a small shift in the angle corresponding to minimum coupling determined by the TDC method away from 90°. This small shift in angle is due to an asymmetry in the transition density when higher order moments are included, which results in a different angle for orthogonality than when considering only dipole moments. When only dipole moments are considered,

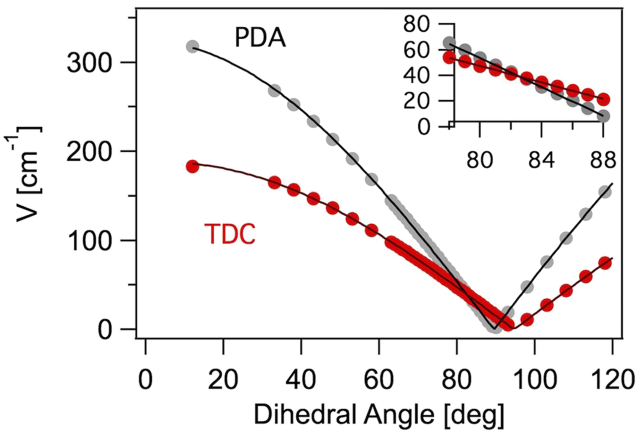

FIG. 3. Electronic coupling between TO molecules intercalated into dsDNA as a function of dihedral angle calculated assuming the point dipole approximation (gray) and using the transition density cube method (red). Solid lines are best fits to $A\,|\cos(\theta + \phi)|$. The inset shows the region of dihedral angles between 78° and 88° where the TDC and PDA curves intersect.

the TDC calculation reproduces the values determined using the PDA.

It is clear that for the coupling strengths present in our TOTO/DNA complex, Fig. 3 inset, the TDC is a small correction to the PDA. This arises due to the near orthogonality between TO molecules. Therefore, the inaccuracies of the PDA estimation of coupling strength as a function of dihedral angle cannot account for the discrepancy between the dihedral angles implied by the RET rates and those implied by the initial and final anisotropy. Prior studies of YOYO, TOTO-3, and TO-PRO-3 suggest that a bound but not fully intercalated subpopulation coexists with the intercalated geometry.[16,41] Significant non-intercalating populations of YOYO have also been observed at dye loading concentrations that are much higher than the 1:1 TOTO:dsDNA concentration used here.[42,43] A small but non-negligible fraction of non-intercalated TOTO may be responsible for the sub-population with low coupling strengths. To address this possibility, we consider a model that consists of two TOTO/dsDNA geometries: one that is fully bis-intercalated and exhibits moderate TO-TO coupling and a second component that has weaker TO-TO coupling, which might arise, e.g., from partially intercalated or groove bound TOTO. This model is applied to simultaneously describe both the initial and final anisotropy values as well as the anisotropy decay dynamics, rather than analyzing the TOTO dimer based on either observable alone, as doing so ignores half of the information provided by the anisotropy dynamics measurement.

Using Monte-Carlo methods, we simulate the effects of two TOTO configurations on the anisotropy dynamics. In the past, similar methods have been applied to examine the effects of orientational inhomogeneities on homo- and hetero-RET.[26,44,45] Here, we simulate the majority of TOTO as intercalated with a minority sub-population that is only bound and not fully intercalated into DNA. For the intercalated TOTO, the donor-acceptor separation is fixed at 9.6 Å, and the dihedral angle determines the anisotropy dynamics. To accommodate a distribution of dihedral angles, we choose random angles from a Gaussian distribution using the mean and standard deviation as parameters in the model. For the non-intercalated subpopulation, the specific binding modes are not known *a priori*. This subpopulation may include a complicated mixture of geometries where only one TO intercalates and the other remains outside of the base-stack as well as groove binding modes where the TOTO is elongated.[16] Geometries where TOTO cross links two dsDNAs are unlikely since that behavior has been observed only at very high concentrations of DNA ~100 μM.[46] Due to the complexity involved in determining the precise geometries associated with these different binding modes, we have instead chosen to approximate their effect through a distribution of static isotropic dipoles where the separation distance (R_b) determines the anisotropy dynamics. While the TDC estimation of the electronic coupling is needed to describe the intercalated TOTO, the PDA is an acceptable approximation for non-intercalating TOTO where the inter-chromophore distance may be ~20 Å, which is approximately the center-to-center distance between TOs when TOTO is elongated. Prior studies have show that the errors introduced by using the PDA are reduced to <5% when orientational averaging is considered for chromophores separated by ~20 Å.[12] We calculate the electronic coupling for each configuration and from it the corresponding anisotropy dynamics using Eq. (2). These dynamics are then averaged across the ensemble. We observe good agreement between the measured and simulated anisotropy dynamics for an ensemble where 80% of the TOTO is intercalated and 20% of the TOTO is bound to the dsDNA, Fig. 4(a). In this representative case, where the dsDNA is 12 bp long and is in PBS buffer, we find that the intercalated fraction has a dihedral angle of 81° with a gaussian standard deviation of 5°, while the bound fraction has a TO-TO (center-center) separation of 19 Å. Ignoring the non-intercalated population underestimates the residual anisotropy observed at longer delays, Fig. 4(a) (blue line). If we average the Monte Carlo simulation results from all of the individual measurements in Fig. S2, we find that 80% of the TOTO intercalates with a mean dihedral angle of 80.7° ± 0.6° and a standard deviation of 4.8° ± 0.4°, and 20% of the TOTO is bound to the dsDNA with a TO-TO separation of 19 ± 1 Å. Treating each of these structures as equivalent is justified by the close agreement among the results of those simulations, which are discussed below. For our TOTO/dsDNA system, the PDA predicts similar anisotropy decay dynamics for the intercalated fraction as the TDC because of their coincidental agreement for a dihedral angle of ~82°.

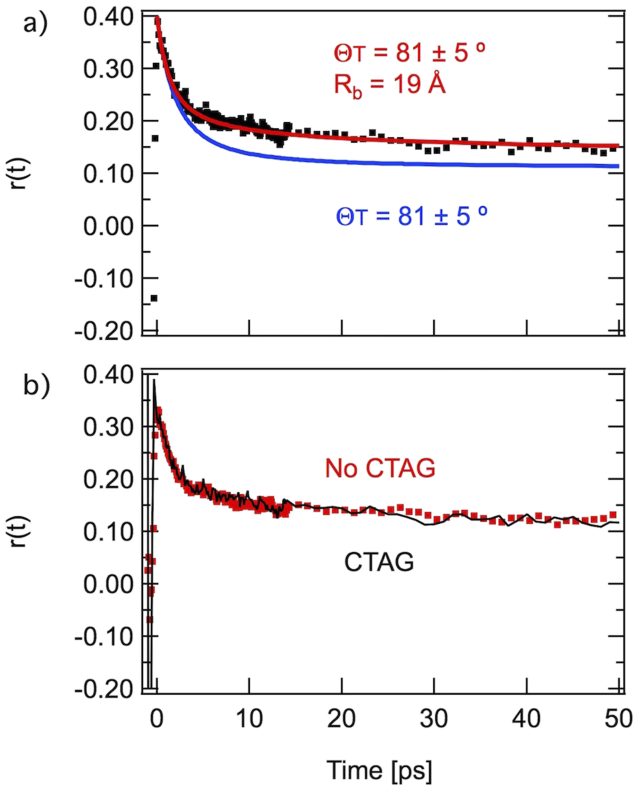

FIG. 4. (a) Comparison between the measured anisotropy dynamics of a 1:1 mixture of TOTO and 12 bp dsDNA in PBS (black, dots) and those simulated assuming the TDC method for an ensemble composed of 100% intercalated TOTO (blue) with a Gaussian distribution of dihedral angles (θ_i) or an ensemble composed of 80% intercalated TOTO and 20% non-intercalated TOTO (red) with isotropic dye orientations and a fixed dye separation (R_b). (b) A comparison between the anisotropy dynamics of 1:1 TOTO:dsDNA for an 18 bp dsDNA duplex without a CTAG present (red) and a 12 bp dsDNA duplex with a CTAG present (black), both in PBS.

Similar anisotropy dynamics and simulation results were observed for TOTO in 12 and 14 base-pair dsDNA, Fig. S2 of the supplementary material. No significant difference in dihedral angle or fraction of non-intercalating TOTO was found between the PBS, TAE, and TAPS buffers. Interestingly, we also examined an 18 bp dsDNA with no CTAG site, Fig. 4(b). Although site specificity no longer exists, we find no significant difference in the anisotropy dynamics and conclude that TOTO intercalates with approximately the same orientation and therefore exhibits the same coupling strength as when the CTAG is present.

To further understand the origin of the non-intercalating subpopulation, we have also examined the effects of changing the TOTO:DNA concentration ratio from 1:5 to 5:1. As TOTO:DNA is increased from 1:5 to 1:1 there is a small but systematic increase in the intensity of the vibronic peak on the absorption band near 490 nm, Fig. S6 of the supplementary material. When excess TOTO is present, i.e., the 2:1 and 5:1 TOTO:DNA ratios, we observe additional modifications of the absorption spectrum, including a further increase in the vibronic peak and a broadening of the full band for the 5:1 ratio. Similar observations have been made for YOYO at high ratios of dye:bp.[42,43] For the lower TOTO:DNA ratios (i.e., 1:5, 1:2, 1:1), the slight increase in the vibronic peak intensity might be an indication of instances in which more than one TOTO binds to DNA. This is consistent with exciton-vibration coupling theory that predicts a redistribution of oscillator strength towards higher energy vibronic transitions as the electronic coupling increases.[47] At the 5:1 ratio, we observe pronounced deviations between the absorption spectrum and fluorescence excitation spectrum consistent with the formation of H-type dimers of TO,[21,22] as shown in Fig. S7 of the supplementary material. In this case, such non-fluorescent dimers could be bound to dsDNA or free in solution. We observe faster fluorescence decay rates at the 2:1 and 5:1 TOTO:DNA ratios, Fig. S6, which is consistent with dynamic quenching observed in YOYO and cyanine dimers.[13,43] Together this suggests that aggregation of the TOTO occurs for high TOTO:DNA ratios, where several TOTO molecules may interact with the DNA, e.g., by groove binding or through multiple intercalated TOTO within the DNA base stack. Both cases could give rise to the observed evidence of strong coupling. Linear and circular dichroism studies suggest that the dominant geometry at these high dye:bp ratios is a groove bound dimer with nearly orthogonal dipoles.[42,43]

By comparison, the anisotropy dynamics show only subtle changes with TOTO:dsDNA ratio, Fig. S8 of the supplementary material. This may arise because the anisotropy is measured for the monomer stimulated emission band, where non-fluorescent dimers may have small contributions due to blue shifted electronic transitions and rapid internal conversion to the ground state. The observed dye loading independence implies that the non-intercalating TOTO represents a significant fraction of the ensemble even for the case of excess DNA. This suggests that the non-intercalating configuration is not the result of a lack of favorable sites for intercalation. Instead, it is more likely that the non-intercalating population arises from a dynamic process by which the TOTO binds to the DNA, intercalates, un-intercalates, and re-enters solution. Indeed, studies of the mechanical properties of bisintercalators have come to a similar conclusion that intercalated geometries are in a dynamic equilibrium with non-intercalating geometries.[16]

The agreement between our simulations and measurements suggests that non-intercalating TOTO may be responsible for the fraction of the ensemble with weak electronic coupling, unfavorable orientations for energy transfer, and slow anisotropy dynamics. This is consistent with recent reports suggesting that a bound but not fully intercalated configuration of YOYO and TO-PRO coexists in a dynamic equilibrium with the intercalated conformation even at low concentrations.[16,41] The subpopulation of non-intercalated orientations gives rise to a distribution of electronic coupling strength that has its peak population with an electronic coupling near zero, a mean value of 14 cm^{-1}, and a half maximum of ~25 cm^{-1}, Fig. 5. The distribution of dihedral angles of the intercalated TOTO is centered at 80.7° ± 0.6°, which is in reasonable agreement with prior estimates of the intercalation geometry based on NMR measurements.[11,17] The 4.8° standard deviation, or 11.3° FWHM, of the distribution of angles seems reasonable for

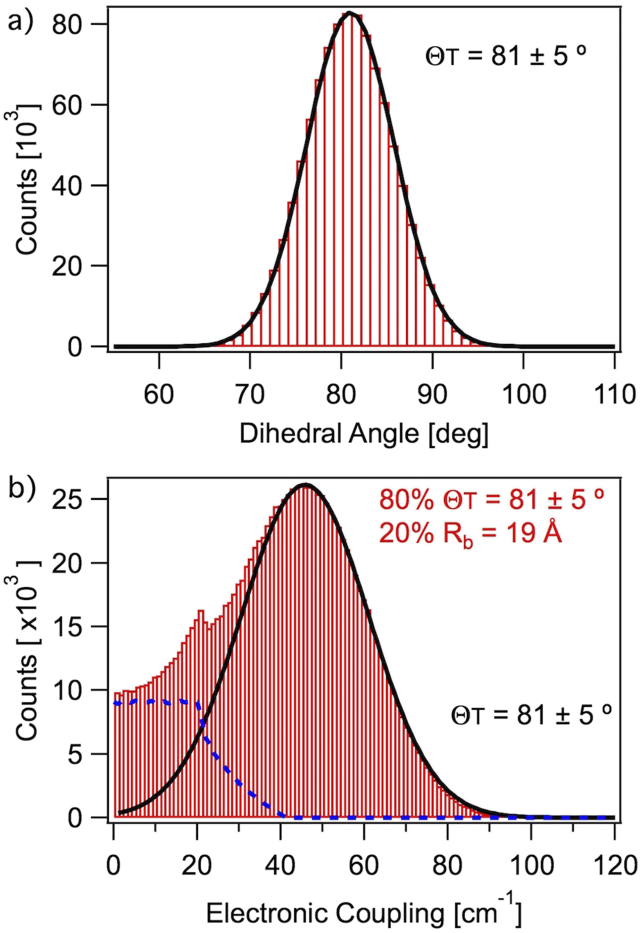

FIG. 5. (a) The Gaussian distribution of the dihedral angles of the intercalated fraction of TOTO. (b) The distribution of electronic coupling strengths associated with an ensemble composed of 80% intercalated TOTO with a Gaussian distribution of dihedral angles (θ_T) and 20% non-intercalated TOTO with isotropic dye orientations and a fixed dye separation (R_b). The black line indicates the contribution from the intercalated fraction. The dashed blue line indicates the contribution from the non-intercalated fraction. The distributions in (a) and (b) result from the average θ_T and R_b from the measurements in Fig. S2 of the supplementary material.

intercalation, which restricts dye motion but does not involve any covalent bonding between dye and DNA to fix the dihedral angle. This results in a distribution of coupling strengths centered at 45 cm^{-1} with a standard deviation of 22 cm^{-1}. The distribution of angles may be a general trait of bis-intercalating cyanine dyes as a similar distribution of dihedral angles has been proposed to describe the anisotropy dynamics observed for YOYO/dsDNA.[17]

It should be pointed out that it is also possible to reproduce the anisotropy measurements by considering a much wider distribution of dihedral angles centered at 84° with FWHM of 23.5°. However, we find that model unsatisfying. The biexponential fits support the idea of two different geometries, giving rise to the observed anisotropy dynamics rather than a single distribution of orientations. The notion of two binding geometries is also consistent with the observation of biexponential TOTO/dsDNA fluorescence decays, where a second component with 10%-18% relative amplitude was needed to reproduce the experimental data. Therefore, we conclude that our model, which includes a small component of non-fully intercalated geometries together with a dominant component that is fully intercalated, is more consistent with our observations.

IV. CONCLUSION

In summary, we have used ultrafast anisotropy measurements to explore the energy transfer properties of the TOTO/DNA complex. We observe biexponential anisotropy relaxation dynamics indicative of two configurations of the TOTO/dsDNA complex: intercalated and non-intercalated TOTO. Although there are only small differences in electronic coupling between the TDC method and PDA for the particular geometries that TOTO assumes, we find that generally the PDA overestimates this value. Based on the application of the TDC method and Monte Carlo simulations, we were able to estimate the dihedral angles of the intercalated TOTO, dye separation of the non-intercalated TOTO, the relative fraction of each subpopulation, and their respective electronic coupling strengths. We find that these properties are insensitive to the presence of a preferential CTAG binding site and show little variation between TAPS, TAE, and PBS buffer solutions. The presence of these two binding modes persists even for low dye loading ratios when there are excess DNA strands and seems to be an intrinsic property of bisintercalation. The orientational inhomogeneities and preferences towards near orthogonal geometries for energy transfer prevent the electronic coupling strength from becoming strong enough to produce bands in the absorption spectrum at room temperature. Finally, the energy transfer rate in TOTO is found to be approximately twice that of YOYO.[17]

Because of the close spacing between dyes, the bis-intercalating TOTO and other structures involving TO dyes intercalated into DNA may present interesting tests of coherent energy transfer effects in synthetic chromophore systems. Interestingly, while the near orthogonal arrangement of the dyes in TOTO/dsDNA limits the electronic coupling strength, it is still similar to the range of electronic coupling between chromophores in some biological light harvesting systems,[48–50] which have shown evidence for quantum coherent effects. Further, by using methods to insert TO as a surrogate nucleobase within the DNA, it may be possible to study coherence effects by tuning the strength of the electronic coupling between TO pairs.[22]

SUPPLEMENTARY MATERIAL

See supplementary material for more details concerning TOTO absorption, fluorescence and fluorescence lifetimes, Monte Carlo simulations of TOTO/dsDNA, transition density cube calculation details, and TOTO and DNA concentration dependent measurements.

ACKNOWLEDGMENTS

This work was supported by the U.S. Naval Research Laboratory (NRL) Nanoscience Institute and the Laboratory University Collaborative Initiative (LUCI) program in support of the VBFF program. Funding for W.P.B. and M.B. has been provided by the Army Research Office MURI Award No. W911NF1210420. W.P.B. and M.B. also acknowledge the Office of Naval Research DURIP Award Nos. N00014-13-1-0664 and N00014-15-1-2830, which funded the high-performance computational cluster in the Bathe laboratory used for the TDC calculations.

[1] H. S. Rye, S. Yue, D. E. Wemmer, M. A. Quesada, R. P. Haughland, R. A. Mathies, and A. N. Glazer, Nucleic Acids Res. **20**, 2803–2812 (1992).
[2] A. N. Glazer and H. S. Rye, Nature **359**, 859–861 (1992).
[3] M. F. Fouz, K. Mukumoto, S. Averick, O. Molinar, B. M. McCartney, K. Matyjaszewski, B. A. Armitage, and S. R. Das, ACS Cent. Sci. **1**, 431–438 (2015).
[4] C. Flors, C. N. J. Ravarani, and D. T. F. Dryden, ChemPhysChem **10**, 2201–2204 (2009).
[5] M. Ganji, S. H. Kim, J. van der Torre, E. Abbondanzieri, and C. Dekker, Nano Lett. **16**, 4699–4707 (2016).
[6] J. G. Woller, J. K. Hannestad, and B. Albinsson, J. Am. Chem. Soc. **135**, 2759–2768 (2013).
[7] J. K. Hannestad, P. Sandin, and B. Albinsson, J. Am. Chem. Soc. **130**, 15889–15895 (2008).
[8] T. L. Netzel, K. Nafisi, M. Zhao, J. R. Lenhard, and I. Johnson, J. Phys. Chem. **99**, 17936–17947 (1995).
[9] J. P. Jacobsen, J. B. Pedersen, L. F. Hansen, and D. E. Wemmer, Nucleic Acids Res. **23**, 753–760 (1995).
[10] J. Bunkenborg, M. M. Stidsen, and J. P. Jacobsen, Bioconjugate Chem. **10**, 824–831 (1999).
[11] H. P. Spielmann, D. E. Wemmer, and J. P. Jacobsen, Biochemistry **34**, 8542–8553 (1995).
[12] A. Munoz-Losa, C. Curutchet, B. P. Krueger, L. R. Hartsell, and B. Mennucci, Biophys. J. **96**, 4779–4788 (2009).
[13] P. D. Cunningham, A. Khachatrian, S. Buckhout-White, J. R. Deschamps, E. R. Goldman, I. L. Medintz, and J. S. Melinger, J. Phys. Chem. B **188**, 14555–14565 (2014).
[14] K. Pan, E. Boulais, L. Yang, and M. Bathe, Nucleic Acids Res. **42**, 2159–2170 (2014).
[15] Z. Zeng, S. M. Clark, R. A. Mathies, and A. N. Glazer, Anal. Biochem. **252**, 110–114 (1997).
[16] D. H. Paik and T. T. Perkins, Angew. Chem., Int. Ed. **51**, 1811–1815 (2012).
[17] A. Fürstenberg, M. D. Julliard, T. G. Deligeorgiev, N. I. Gadjev, A. A. Vasilev, and E. Vauthey, J. Am. Chem. Soc. **128**, 7661–7669 (2006).
[18] H. M. Berman, J. Westbrook, Z. Feng, G. Gililand, T. N. Bhat, H. Weissig, I. N. Shindyalov, and P. E. Bourne, Nucleic Acids Res. **28**, 235–242 (2000).
[19] S. A. Diaz, S. Buckhout-White, M. G. Ancona, C. M. Spillmann, E. R. Goldman, J. S. Melinger, and I. L. Medintz, Adv. Opt. Mater. **4**, 399–412 (2016).
[20] P. D. Cunningham, K. M. McCreary, A. T. Hanbicki, M. Currie, B. T. Jonker, and L. M. Hayden, J. Phys. Chem. C **120**, 5819–5826 (2016).

[21] S. Berndl, S. D. Dimitrov, F. Menacher, T. Fiebig, and H.-A. Wagenknecht, Chem. - Eur. J. **22**, 2386–2395 (2016).
[22] H. Asanuma, T. Fujii, T. Kato, and H. Kashida, J. Photochem. Photobiol., C **13**, 124–135 (2012).
[23] J. Lakowicz, *Principles of Fluorescence Spectroscopy*, 2nd ed. (Klumer Academic/Plenum Publishers, New York, 1999).
[24] P. D. Cunningham, J. E. Boercker, D. Placencia, and J. G. Tischler, ACS Nano **8**, 581–590 (2014).
[25] S. Sindbert, S. Kalinin, H. Nguyen, A. Kienzler, L. Clima, W. Bannwarth, B. Appel, S. Muller, and C. A. M. Seidel, J. Am. Chem. Soc. **133**, 2463–2480 (2011).
[26] J. S. Melinger, A. Khachatrian, M. G. Ancona, S. Buckhout-White, E. R. Goldman, C. M. Spillmann, I. L. Medintz, and P. D. Cunningham, ACS Photonics **3**, 659–669 (2016).
[27] M. N. Berberan-Santos and B. Valeur, J. Chem. Phys. **95**, 8048–8055 (1991).
[28] G. D. Scholes, Annu. Rev. Phys. Chem. **54**, 57–87 (2003).
[29] T. Förster, Ann. Phys. **437**, 55–75 (1948).
[30] B. W. van der Meer, D. M. van der Meer, and S. S. Vogel, in *FRET–Förster Resonance Energy Transfer: From Theory to Applications*, edited by I. L. Medintz and N. Hildebrandt (Wiley-VCH, 2013).
[31] H. Ihmels and D. Otto, Top. Curr. Chem. **258**, 161–204 (2005).
[32] B. P. Krueger, G. D. Scholes, and G. R. Fleming, J. Phys. Chem. B **102**, 5378–5386 (1998).
[33] W. P. Bricker and C. S. Lo, J. Phys. Chem. B **118**, 9141–9154 (2014).
[34] W. Kohn and L. J. Sham, Phys. Rev. **140**, A1133–A1138 (1965).
[35] E. Runge and E. K. U. Gross, Phys. Rev. Lett. **52**, 997 (1984).
[36] T. Yanai, D. P. Tew, and N. C. Handy, Chem. Phys. Lett. **393**, 51–57 (2004).
[37] R. Ditchfield, W. J. Hehre, and J. A. Pople, J. Chem. Phys. **54**, 724–728 (1971).
[38] W. J. Hehre, R. Ditchfield, and J. A. Pople, J. Chem. Phys. **56**, 2257–2261 (1972).
[39] M. Valiev, E. J. Bylaska, N. Govind, K. Kowalski, T. P. Straatsma, H. J. J. Van Dam, D. Wang, J. Nieplocha, E. Apra, T. L. Windus, and W. A. de Jong, Comput. Phys. Commun. **181**, 1477–1489 (2010).
[40] A. Bakan, L. M. Meireles, and I. Bahar, Bioinformatics **27**, 1575–1577 (2011).
[41] N. Milanovich, M. Suh, R. Jankowiak, G. J. Small, and J. M. Hayes, J. Phys. Chem. **100**, 9181–9186 (1996).
[42] A. Larsson, C. Carlsson, M. Jonsson, and B. Albinsson, J. Am. Chem. Soc. **116**, 8459–8465 (1994).
[43] S. G. Lopez, M. J. Ruedas-Rama, S. Casares, J. M. Alvarez-Pez, and A. Orte, J. Phys. Chem. B **116**, 11561–11569 (2012).
[44] M. Hoefling, N. Lima, D. Haenni, C. A. M. Seidel, B. Schuler, and H. Grubmüller, PLoS One **6**, e19791 (2011).
[45] S. S. Vogel, T. A. Nguyen, B. W. van der Meer, and P. S. Blank, PLoS One **7**, e49593 (2012).
[46] C. Carlsson, M. Jonsson, and B. Åkerman, Nucleic Acids Res. **23**, 2413–2420 (1995).
[47] S. Polyutov, O. Kühn, and T. Pullerits, Chem. Phys. **394**, 21–28 (2012).
[48] G. S. Engel, T. R. Calhoun, E. L. Read, T.-K. Ahn, T. Mancal, Y.-C. Cheng, R. E. Blankenship, and G. R. Fleming, Nature **446**, 782–786 (2007).
[49] R. Hildner, D. Brinks, J. B. Nieder, R. J. Cogdell, and N. F. van Hulst, Science **340**, 1448–1451 (2013).
[50] F. P. Diehl, C. Roos, A. Duymasz, B. Lunkenheimer, A. Köhn, and T. Basché, J. Phys. Chem. Lett. **5**, 262–269 (2014).